Scientific Research Publishing

Open Journal of Fluid Dynamics, 2025, 15(2), 64-86
https://www.scirp.org/journal/ojfd
ISSN Online: 2165-3860
ISSN Print: 2165-3852

Combined Effects of Magnetic Field and Nanoparticles on Rotating Engine-Oil Flow Using a New Local Thermal Non-Equilibrium Formulation

Sèmako Justin Dèdèwanou[1,2*], Thierno Mamadou Pathé Diallo[1], Mamadou Billo Doumbouya[1], Mariama Ciré Sylla[1], Facinet Camara[1], Amoussou Laurent Hinvi[2,3]

[1]Laboratoire de Recherche Appliquée en Sciences de la Nature (LARASCINA), Département de Physique, Faculté des Sciences, Université de Kindia (UK), Kindia, Guinée
[2]Laboratoire de Mécanique des Fluides, de la Dynamique Nonlinéaire et de la Modélisation des Systèmes Biologiques (LMFDNMSB); Institut de Mathématiques et de Sciences Physiques (IMSP), Porto-Novo, Bénin
[3]Laboratoire des Procédés et de l'Innovation Technologique (LaPIT), Université Nationale des Sciences, Technologie, Ingénierie et Mathématiques (UNSTIM), Abomey, Bénin
Email: *justin.dedewanou@imsp-uac.org

How to cite this paper: Dèdèwanou, S.J., Diallo, T.M.P., Doumbouya, M.B., Sylla, M.C., Camara, F. and Hinvi, A.L. (2025) Combined Effects of Magnetic Field and Nanoparticles on Rotating Engine-Oil Flow Using a New Local Thermal Non-Equilibrium Formulation. *Open Journal of Fluid Dynamics*, **15**, 64-86.
https://doi.org/10.4236/ojfd.2025.152005

Received: April 18, 2025
Accepted: May 25, 2025
Published: May 28, 2025

Abstract

Engine oil is a liquid used in a wide range of applications, as it is an essential lubricant, but it also cools, washes and helps prolong the performance of industrial machinery, vehicle engines and aircraft combustion treatment. This paper deals with the (alumina-tantalum)/engine oil hybrid nano-liquid flow in a porous medium subjected to rotational and Lorenz forces. We have used the Darcy-Bénard convection model for the momentum equation and a new local thermal non-equilibrium formulation for heat transport. Linear stability theory and non-linear stability theory based on the minimal double Fourier series representation are used to study the appearance of stationary and chaotic convection in the hybrid nano-liquid. The analytical expression of the stationary thermal Rayleigh-Darcy number has been found to be a function of the parameters and physicochemical properties of the nano-liquid. In addition, a robust 6-dimensional nonlinear system was determined for the study of chaotic convection. The effects of dimensionless parameters and nanofragments were analyzed graphically. The added value of this work lies in stabilizing and controlling the onset of thermal instability and chaotic convection in engine oil by adding alumina-tantalum nanofragments and applying a magnetic field and/or a rotational force.

Keywords

Engine-Oil, LTNE Formulation, Thermal Instability, Chaos

1. Introduction

Heat transport is a concept used in physics and engineering and is involved in many areas of our daily lives, including the design of cooling systems, thermodynamics, cooking, mechanical engineering, materials science, heating, refrigeration, energy optimization and more [1] [2]. Efficient heat transfer in these industrial operations is a fundamental requirement for all processes involving thermal convection. The addition of one or more nanofragments to ordinary liquids to obtain mono- or hybrid nanoliquids is a promising alternative solution for improving the thermal properties of said base liquid. Motor oil is used as a lubricant and coolant in engines and industrial activities. It is one of the basic liquids used in combustion engines, solar energy, oil refineries, heat exchangers, and many other industrial fields. Applications of crossed hybrid triadic nanofragments suspended in engine oil by quadratic and regular convection with magnetic dipole were presented by Wang in [3]. They found that hybrid nanoparticles improved thermal performance more than mono-nanoparticles. An entropy optimization approach is used by Afzal in [4] to show the heat transfer enhancement in engine oil-based hybrid nanofluid through combustive engines. They revealed that increasing the magnetic field strength decreases the velocity of the engine oil nanofluid hybrid. An experimental study of thermal convection in a rectangular engine oil tank heated from below was carried out by Ayed in [5] [6]. The process of thermal convection in porous media is a very active area of research due to the thermal behavior of fluids in technical applications to meet various specifications, such as preserving fluid characteristics over a wide range of temperatures and stresses like thermal reservoirs [7]. Rayleigh-Benard convection in porous media is classified into two categories: Darcy-Benard convection when the medium's porosity is low, and Brinkman-Benard convection when the medium's porosity is high. In a fluid-saturated porous medium, it is well known that the Darcy-Rayleigh number is used to characterize the start of convective transport. These convective motions have been the subject of several studies using Fourier's heat flux law to model the energy equation in [8]-[13] and others. Turkyilmazoglu presented the influences of Brinkman-Darcy-Bénard model on the onset of free convection inside an impermeable porous channel with imposed isoflux thermal constraints in [14]. He also showed in [15] that a linear stability analysis is always accessible by successively orienting the vortex disturbance, thus enabling us to investigate the conditions for the onset of convective instability. Furthermore, there is an ambiguity concerning the parabolic nature of Fourier's simple law of heat transfer. In applications using Fourier's law, the assumption is that heat transfer occurs instantaneously in the medium as soon as a temperature gradient appears. Such a heat

propagation law may be physically acceptable when there is no phase shift caused by a mechanism in the medium. This Fourier law predicts an infinite speed of heat propagation, and this drawback makes it unsuitable for many current problems in which new thermal situations arise due to the increasing use of new materials. A new law with a phase shift is needed to predict the finite speed of heat transfer in such application situations; this leads to the introduction of the hyperbolic heat equation. It resists the law of causality for the propagation of thermal waves in macroscopic bodies. When a small thermal offset is incorporated into the heat propagation equation, the result is thermal disturbances that can travel at finite speed as waves. Straughan was the first to apply Cattaneo's law of heat flux to the problem of thermal convection in a viscous fluid [16]. Later, Joseph revised and interpreted the concept of heat transmission by waves in [17], while introducing the notion of effective heat capacity, relaxation functions and effective thermal conductivity for heat and energy along lines used recently to describe the elastic response of viscous liquids. They found the redeveloped expression of the heat flux vector field concerning the thermal offset. The unfeasible characteristic of the thermal wave is eliminated by the Maxwell-Cattaneo principle with circulation at infinite speed, but it leads to a contradiction of causality in the continuum. This Maxwell-Cattaneo principle is based on the reference frame of motion of objects. To resolve this paradox, Christov proposed a generalization of Fourier's principle in [18] that does not vary according to the frame of reference. All the ambiguities of heat transfer in the continuum are almost resolved by the application of the convective derivative. However, this modified law produces multiple equations for the temperature field. To remove this unpleasant behavior of the heat flow principle, a different frame-invariant formalism, considering Oldroyd's higher time convective derivative operator instead of the partial derivative operator, was devised by Christov in [19]. This objective immutable modification sorts out all the ambiguous features of thermal wave propagation and produces a unique equation for the temperature field by eliminating the heat flux vector. However, the thermal time lag should be small enough to obey the continuum's hypothetical limitations. Straughan exploited this new law in [20] to investigate the stability analysis of the convective flow of viscous liquid in non-porous medium. The results of this study revealed that when the Cattaneo number becomes significant, the instability from stationary to oscillatory convective transport. He also studied the problem of thermo-convection in a porous Darcy material saturated with a Newtonian fluid using the Cattaneo heat flux [21]. He noted that at the threshold Cattaneo number, convection changes from a steady state to an oscillatory state and that the wave number increases discontinuously, meaning that convective cells have a narrower hexagonal shape.

Furthermore, when there is a mismatch between the thermal properties of the fluid and those of the porous matrix, a shift in the thermal transaction between the two phases of local thermal non-equilibrium occurs, enabling a new formulation to be considered. Straughan used a new law of flux of heat (local temperatures of thermal non-equilibrium with Cattaneo model) to study thermal convection in

a fluid-saturated porous Darcy medium [22]. He found a new system of partial differential equations involving Darcy's law, a parabolic equation of the fluid temperature and, effectively, a hyperbolic equation of the solid skeleton temperature. In some modern industrial operations described by Dehghan in [23], local thermal non-equilibrium must be taken into account. Shi presented in [24] a new criterion for estimating local thermal non-equilibrium conditions for heat transport in porous aquifers. They emphasized that LTNE effects must be taken into account when using heat as a tracer to quantify bed fluxes and thermal properties of saturated stream sediments in the presence of low Darcian velocities and large particle sizes. Also, Al-Sumaily has carried out [25] a comprehensive review of the legitimacy of the assumption of local thermal equilibrium in porous media. They reported that it is not prudent to increase the porosity or particle diameter of packed beds or the amplitude and/or frequency when imposing a thermal perturbation on the system. They also revealed that the results showed contradictory conclusions on the effects of certain relevant parameters in certain physical cases.

The general criterion of local thermal non-equilibrium (LTNE) and the influence of nanoparticles in base fluids were examined by Prasannakumara [26] in the case of heat transfer from a nanoliquid flow over a stretched sheet in a porous medium. They concluded that increasing the heat transfer parameter between phases led to a decrease in the fluid phase heat transfer rate and an increase in the solid phase heat transfer rate. Agarwal studied the effect of local thermal non-equilibrium on linear thermal instability in a horizontal layer of a Newtonian nanofluid [27]. They found that convection sets in earlier for LTNE than for LTE, and that the rate of mass and heat transfer increases with the value of the thermal Rayleigh number. Kasaeian and his colleagues reviewed the latest developments on nanofluid flow and heat transfer in porous media [28].

Recently, Siddheshwar derived in [29] a new type of thermal equation for the phase-shifting effects that occur naturally in the heat transfer problem without thermal equilibrium between liquid and solid phases to study the occurrence of regular and chaotic Darcy-Benard convection in a porous medium-saturated with an ordinary fluid. The aim of this work is to extend this model to the case of hybrid nanofluids, choosing motor oil as the base liquid and alumina-tantalum nanoparticles by considering the combined effects of rotational force and Lorenz force satisfying Maxwell's, Ampère's and Faraday's laws. The novelty of this work is that all analytical expressions of the stationary thermal Rayleigh-Darcy number for the linear analysis and the 6-dimensional system of nonlinear equations found are functions of the physico-chemical parameters of the hybrid nanoliquid (engine oil + nanofragments), enabling effective and efficient prediction of the thermal and dynamic behaviors of the engine oil flow.

2. Mathematical Modeling

2.1. Problem Formulation

A rectangular porous cavity saturated with (alumina-tantalum)/motor oil is con-

sidered. The top and bottom walls are kept at constant temperatures T_0 and $T_0+\Delta T$, respectively. The Cartesian coordinate system used is composed of the unit vectors $\boldsymbol{e}_x$, $\boldsymbol{e}_y$ and $\boldsymbol{e}_z$, whose y-axis follows the horizontal and vertical z-axis is collinear with gravity. The porous medium is subjected to a uniform magnetic field $\boldsymbol{B}_0$. For this problem, we have neglected the effect of Joule heat and viscous dissipation on heat transfer, and have assumed that the induced magnetic field is very weak compared with $\boldsymbol{B}_0$.

Referring to the work of Dèdèwanou in [30] [31], of Cimpean in [32] and of Manjunatha in [33], taking into account the above-mentioned criteria and assuming local thermal non-equilibrium between the liquid and solid phases of the skeleton in the porous medium, the coupled equations governing the convective flow of the hybrid nanoliquid are modeled as follows:

$$\nabla\cdot\boldsymbol{q}=0, \tag{1}$$

$$\begin{aligned}&\frac{\rho_{hnf}}{\varepsilon}\left[\frac{\partial\boldsymbol{q}}{\partial t}+\frac{1}{\varepsilon}(\boldsymbol{q}\cdot\nabla)\boldsymbol{q}\right]\\&=-\nabla P-\rho\boldsymbol{g}+\frac{\mu_{hnf}}{\varepsilon}\nabla^2\boldsymbol{q}-\frac{\mu_{hnf}}{K}\boldsymbol{q}+\frac{2\rho_{hnf}}{\varepsilon}(\boldsymbol{q}\wedge\boldsymbol{\Omega})+\sigma_{hnf}\boldsymbol{J}\wedge\boldsymbol{B}_0,\end{aligned} \tag{2}$$

$$(\rho Cp)_{hnf}\left[\varepsilon\frac{\partial T}{\partial t}+(\boldsymbol{q}\cdot\nabla)T\right]=\varepsilon k_{hnf}\nabla^2T+Q(T-T_0), \tag{3}$$

$$(1-\varepsilon)(\rho Cp)_s\frac{\partial T_s}{\partial t}=(1-\varepsilon)k_s\nabla^2T_s+Q(T_s-T). \tag{4}$$

The nano-liquid considered complies with Faraday's law, Ampere's law, Maxwell's law and the Gauss equations defined as:

$$\nabla\wedge\boldsymbol{B}_0=\mu_e(\boldsymbol{J}+\varepsilon_e\boldsymbol{E}), \tag{5}$$

$$\nabla\wedge\boldsymbol{E}=-\frac{\partial\boldsymbol{B}_0}{\partial t}, \tag{6}$$

$$\nabla\cdot\boldsymbol{B}_0=0, \tag{7}$$

$$\nabla\cdot\boldsymbol{E}=0, \tag{8}$$

$$\nabla\cdot\boldsymbol{J}=0, \tag{9}$$

with

$$\boldsymbol{J}=\sigma_{hnf}(\boldsymbol{E}+\boldsymbol{v}\wedge\boldsymbol{B}_0) \tag{10}$$

and μ_e, ε_e are the magnetic permeability and absolute permeability of the fluid respectively.

In the above equations, $\nabla=\frac{\partial}{\partial x}\boldsymbol{e}_x+\frac{\partial}{\partial y}\boldsymbol{e}_y+\frac{\partial}{\partial z}\boldsymbol{e}_z$ is the gradian vector and $\nabla^2=\frac{\partial^2}{\partial x^2}+\frac{\partial^2}{\partial y^2}+\frac{\partial^2}{\partial z^2}$ is the Laplacian operator. The indices hnf, f and s represent the properties of the nanoliquid, base liquid and solid respectively.

Given the extremely small size of the nanofragments, the interaction between the heat transfer fluid and the nanoparticles does not generate extracorporeal

torque or other forces. It simply modifies the spatio-temporal properties, which are obtained from experimental data. Adopting the Boussinesq approximation, the equation of state in terms of density at temperature T of the nano-liquid is written as follows:

$$\rho = \rho_{hnf}\left[1-\beta_{hnf}\left(T-T_0\right)\right]. \tag{11}$$

The physico-chemical parameters of the hybrid nano-liquids are

Density:

$$\rho_{hnf} = \varphi_1\rho_1 + \varphi_2\rho_2 + \left(1-\varphi_1-\varphi_2\right)\rho_f, \tag{12}$$

Thermal expansion coefficient:

$$\left(\rho\beta\right)_{hnf} = \varphi_1\left(\rho\beta\right)_1 + \varphi_2\left(\rho\beta\right)_2 + \left(1-\varphi_1-\varphi_2\right)\left(\rho\beta\right)_f. \tag{13}$$

Heat capacitance:

$$\left(\rho Cp\right)_{hnf} = \varphi_1\left(\rho Cp\right)_1 + \varphi_2\left(\rho Cp\right)_2 + \left(1-\varphi_1-\varphi_2\right)\left(\rho Cp\right)_f. \tag{14}$$

Thermal conductivity:

$$\begin{aligned}\frac{k_{hnf}}{k_f} = &\left\{\frac{\varphi_1k_1+\varphi_2k_2}{\varphi_1+\varphi_2} + 2k_f + 2\left(\varphi_1k_1+\varphi_2k_2\right) - 2\left(\varphi_1+\varphi_2\right)k_f\right\}\\ &\times\left\{\frac{\varphi_1k_1+\varphi_2k_2}{\varphi_1+\varphi_2} + 2k_f - \left(\varphi_1k_1+\varphi_2k_2\right) + \left(\varphi_1+\varphi_2\right)k_f\right\}^{-1}.\end{aligned} \tag{15}$$

Dynamic viscosity:

$$\mu_{hnf} = \mu_f\left(1-\varphi_1-\varphi_2\right)^{-2.5}. \tag{16}$$

Electrical conductivity:

$$\sigma_{hnf} = \left\{1+\frac{3\left[\frac{\varphi_1\sigma_{s1}+\varphi_2\sigma_{s2}}{\sigma_{hf}} - \left(\varphi_1+\varphi_2\right)\right]}{\left[\frac{\varphi_1\sigma_{s1}+\varphi_2\sigma_{s2}}{\sigma_{hf}\left(\varphi_1+\varphi_2\right)} + 2\right] - \left[\frac{\varphi_1\sigma_{s1}+\varphi_2\sigma_{s2}}{\sigma_{hf}} - \left(\varphi_1+\varphi_2\right)\right]}\right\}\sigma_{hf}. \tag{17}$$

Subscripts 1 and 2 refer to aluminate and tantalum nanoparticles respectively. The porous medium thermal conductivity saturated with hybrid nanoliquid is [34]:

$$k_{mhnf} = \varepsilon k_{hnf} + \left(1-\varepsilon\right)k_s. \tag{18}$$

Note that above 4% nanofragments volume fraction, the nanofluid becomes a non-Newtonian fluid, which would lead to a significant increase in viscosity and cancel out any benefit obtained in terms of improved thermal conductivity.

The porous medium saturated with nanoliquids occupies the domain $\Omega = \left\{\left(x,y,z\right)\in\mathbb{R}^3\right\}\times\left\{y\in\left(0,l\right)\right\}\times\left\{z\in\left(0,h\right)\right\}$. The nanoliquid flow is such that the convective rolls have axes parallel to the shortest dimension, *i.e.*, the velocity component along the x-axis is zero. Thus, the equations governing nanofluid flow are reduced to 2-D. The stress-free and slip-free boundary conditions with the perturbation technique for the nanofluid flow problem are described as follows:

$$\left.\begin{array}{ll} T = T_s = T_0 + \Delta T & \text{at } z = 0 \\ T = T_s = T_0 & \text{at } z = h \\ \boldsymbol{q} = \boldsymbol{0} & \text{at } z = 0, h \end{array}\right\} \tag{19}$$

The Darcy-Benard convective transport model is adopted, assuming low porosity. So, the non-linear terms $(\boldsymbol{q}\cdot\boldsymbol{\nabla})\boldsymbol{q}$ and $\boldsymbol{\nabla}^2\boldsymbol{q}$ are negligible as the porosity of the medium is considered low. By non-dimensionalizing the transport and heat transfer equations using the following quantities

$$Y = \frac{y}{h}, \quad Z = \frac{z}{h}, \quad \tau = \frac{\alpha_w t}{h^2}, \quad V = \frac{hv}{\alpha_w}, \quad W = \frac{hw}{\alpha_w}, \tag{20}$$

$$\tilde{p} = \frac{Kp}{\mu_f \alpha_w}, \quad \Theta = \frac{T}{\Delta T}, \quad \Theta_s = \frac{T_s}{\Delta T}, \tag{21}$$

Pressure is eliminated in Equation (2). Thus, the vorticity transport equation is obtained after subtracting the resulting non-dimensional equations. The coupled partial equations are as follows:

$$\frac{\partial V}{\partial Y} + \frac{\partial W}{\partial Z} = 0 \tag{22}$$

$$\begin{aligned} &\left[\left(\frac{\rho_{hnf}}{\rho_f}\right)\left(\frac{\mu_f}{\mu_{hnf}}\right)\frac{1}{Va}\frac{\partial}{\partial t} + 1\right]\nabla^2 W \\ &= \left(\frac{\mu_f}{\mu_{hnf}}\right)\left(\frac{(\rho\beta)_{hnf}}{(\rho\beta)_f}\right)Ra_f\frac{\partial^2\Theta}{\partial Y^2} + \left(\frac{\rho_{hnf}}{\rho_f}\right)\left(\frac{\mu_f}{\mu_{hnf}}\right)\sqrt{Ta_D}\frac{\partial\zeta}{\partial z} \\ &- \left(\frac{\sigma_{hnf}}{\sigma_f}\right)\left(\frac{\mu_f}{\mu_{hnf}}\right)Ha^2\nabla^2 W, \end{aligned} \tag{23}$$

$$\begin{aligned} &\frac{(\rho Cp)_{hnf}}{(\rho Cp)_f}\left[V_N\frac{\partial\Theta}{\partial\tau} + \frac{\gamma+1}{\gamma}\left(V\frac{\partial\Theta}{\partial Y} + W\frac{\partial\Theta}{\partial Z}\right)\right] \\ &= \frac{k_{hnf}}{k_f}\left(\frac{\partial^2\Theta}{\partial Y^2} + \frac{\partial^2\Theta}{\partial Z^2}\right) - Q_0\left(\Theta - \Theta_s\right), \end{aligned} \tag{24}$$

$$V_N B_N \frac{\partial\Theta_s}{\partial\tau} = \left(\frac{\partial^2\Theta_s}{\partial Y^2} + \frac{\partial^2\Theta_s}{\partial Z^2}\right) - \gamma Q_0\left(\Theta_s - \Theta\right). \tag{25}$$

The vorticity ζ verifies the equation:

$$\begin{aligned} &\left[\left(\frac{\rho_{hnf}}{\rho_f}\right)\left(\frac{\mu_f}{\mu_{hnf}}\right)\frac{1}{Va}\frac{\partial}{\partial t} + \left(1 + \left(\frac{\sigma_{hnf}}{\sigma_f}\right)\left(\frac{\mu_f}{\mu_{hnf}}\right)Ha_f^2\right)\right]\zeta \\ &= \left(\frac{\rho_{hnf}}{\rho_f}\right)\left(\frac{\mu_f}{\mu_{hnf}}\right)\sqrt{Ta_D}\frac{\partial w}{\partial z}. \end{aligned} \tag{26}$$

From Equations (23) and (26), we obtain:

$$\left[\left(\frac{M_1}{Va}\frac{\partial}{\partial t} + M_0\right)^2\nabla^2 + M_1^2 Ta_D\frac{\partial^2}{\partial z^2}\right]W = M_3 Ra_{Df}\left(\frac{M_1}{Va}\frac{\partial}{\partial t} + M_0\right)\frac{\partial^2\Theta}{\partial Y^2}. \tag{27}$$

In Equations (22)-(25), Va is the Vadasz number, Ra_{Df} is the thermal Darcy-

Rayleigh number, Q_0 is the coefficient of scaled inter-phase heat transport, γ is the ratio of porosity-weighted conductivity, V_N is the Vafai number and B_N is the Barletta number expressed as:

$$\begin{aligned}
&Va=\frac{\varepsilon\mu_f h^2}{\rho_f\alpha_w K},\quad Ra_f=\frac{\rho_f g\beta_f hK(\Delta K)}{\alpha_f\mu_f}\left(\frac{k_f}{k_w}\right),\quad Q_0=\frac{Qh^2}{\varepsilon k_f},\\
&\gamma=\frac{\varepsilon k_f}{(1-\varepsilon)k_s},\quad V_N=\frac{\alpha_w}{\alpha_f},\quad B_N=\frac{\alpha_f}{\alpha_s},\quad \alpha_w=\frac{k_w}{(\rho Cp)_w},\\
&\alpha_s=\frac{k_s}{(\rho Cp)_s},\quad Ta_D=\left(\frac{2\Omega\rho_f K}{k\mu_f}\right)^2,\quad M_0=\left(1+M_2 Ha_f^2\right),\\
&M_1=\left(\frac{\rho_{hnf}}{\rho_f}\right)\left(\frac{\mu_f}{\mu_{hnf}}\right),\quad M_2=\left(\frac{\sigma_{hnf}}{\sigma_f}\right)\left(\frac{\mu_f}{\mu_{hnf}}\right),\quad \alpha_f=\frac{k_f}{(\rho Cp)_f},\\
&M_3=\left(\frac{\mu_f}{\mu_{hnf}}\right)\left(\frac{(\rho\beta)_{hnf}}{(\rho\beta)_f}\right),\quad M_4=\left(\frac{(\rho Cp)_f}{(\rho Cp)_{hnf}}\right)\left(\frac{k_{hnf}}{k_f}\right).
\end{aligned}\tag{28}$$

The boundary conditions to which the equations governing nanoliquids in non-dimensional form are subject are defined by:

$$\left.\begin{aligned}
&W=0,\quad \Theta=0,\quad \Theta_s=1\quad \text{at } Z=0,\\
&W=0,\quad \Theta=0,\quad \Theta_s=0\quad \text{at } Z=1.
\end{aligned}\right\}\tag{29}$$

In the basic state, heat is transported only by conduction, and physical quantities vary only along the Y axis, as follows:

$$V_b=0,\quad W_b=0,\quad \Theta=\Theta_b(Z)\quad \text{and}\quad \Theta=\Theta_{sb}(Z)\tag{30}$$

Using the conduction solutions defined in Equation (30), Equations (22)-(25) generate other equations that are solved with the boundary conditions of Equation (29); we obtain

$$\Theta_b(Z)=1-Z\quad \text{and}\quad \Theta_{sb}(Z)=1-Z.\tag{31}$$

Equation (31) shows that the solid and nanoliquid temperatures have the same expression and do not depend on Q_0 and γ, confirming that the basic state is a conduction state. After having carried out small disturbances of the basic flow, which are:

$$\left.\begin{aligned}
&V=V'(\tau,Y,Z),\quad W=W'(\tau,Y,Z),\\
&\Theta=\Theta_b(Z)+\Theta'(\tau,Y,Z)\quad \text{and}\quad \Theta_s=\Theta_b(Z)+\Theta'(\tau,Y,Z).
\end{aligned}\right\}\tag{32}$$

From Equation (32), the equations of motion and heat-flux in the perturbed state take the following form, after omitting prime numbers and neglecting a perturbed quantity for simplicity:

$$\left[\left(\frac{M_1}{Va}\frac{\partial}{\partial t}+M_0\right)^2\nabla^2+M_1^2 Ta_D\frac{\partial^2}{\partial z^2}\right]W=M_3 Ra_D\left(\frac{M_1}{Va}\frac{\partial}{\partial t}+M_0\right)\frac{\partial^2\Theta}{\partial Y^2}\tag{33}$$

$$V_N\frac{\partial\Theta}{\partial\tau}+\frac{\gamma+1}{\gamma}\left[\left(V\frac{\partial}{\partial Y}+W\frac{\partial}{\partial Z}\right)\Theta-W\right]=M_4\left(\frac{\partial^2\Theta}{\partial Y^2}+\frac{\partial^2\Theta}{\partial Z^2}\right)-Q_0(\Theta-\Theta_s),\tag{34}$$

$$V_N B_N \frac{\partial \Theta_s}{\partial \tau} = \left(\frac{\partial^2 \Theta_s}{\partial Y^2} + \frac{\partial^2 \Theta_s}{\partial Z^2} \right) + \gamma Q_0 \left(\Theta - \Theta_s \right). \tag{35}$$

In the absence of nano-fragments ($\varphi = 0$), the nanoliquid parameters M_1, M_2, M_3 and M_4 are all equal to 1. The above condition reduces to governing equations in the perturbed state for simple viscous fluid flow.

2.2. Novel Model of LTNE Heat Equation for Newtonian Nanoliquid

After decoupling the temperatures Θ and Θ_s from Equations (34) and (35), we obtain a new local thermal non-equilibrium equation with three phase shifts:

$$\begin{aligned} &\left(1 + C_{PV} \frac{\partial}{\partial \tau}\right) \frac{\partial \Theta}{\partial \tau} + \left[1 - \frac{1}{\gamma Q_0} \nabla^2 + C_{DN} \frac{\partial}{\partial \tau}\right] \left[\left(V \frac{\partial}{\partial Y} + W \frac{\partial}{\partial Z}\right) \Theta - W\right] \\ &= M_4 \left[1 - \frac{1}{Q_0 (1+\gamma)} \nabla^2 + C_{BS} \frac{\partial}{\partial \tau}\right] \nabla^2 \Theta, \end{aligned} \tag{36}$$

The new parameters of the equation are expressed as follows:

$$C_{PV} = \frac{V_N B_N}{(\gamma + B_N) Q_0}, \; C_{DN} = \frac{V_N B_N}{\gamma Q_0} \text{ and } C_{BS} = \frac{V_N (1 + B_N)}{(1+\gamma) Q_0}. \tag{37}$$

In Equation (36), when Q_0 and γQ_0 respectively tend towards 1, the parameters C_{PV}, C_{DN}, C_{BS} and the theme $\frac{1}{\gamma Q_0}$ tend towards zero. Under this condition, Equation (36) reduces to that of the heat flux according to Fourier's law (local thermal equilibrium) found in [30]. Moreover, in the case where the constants γ and Q_0 have finite values, we obtain an equation that has the characteristics of the hyperbolic heat equation derived from Cattaneo's flux law. The parameters C_{PV}, C_{DN}, C_{BS} correspond to the relaxation/delay times caused by the phase shifts between the relevant quantities. To better understand the pathways leading to local thermal equilibrium from the local thermal non-equilibrium formulation, we introduce Rees numbers into the Darcy Bénard convection problem with LTNE defined as follows:

$$\gamma Q_0 = R_N \cos(\xi), \; Q_0 = R_N \sin(\xi) \tag{38}$$

with the effective thermal resistance of the medium

$$R_N = h^2 Q \sqrt{\left(R_l^2 + R_s^2\right)} \tag{39}$$

and the other Rees number $\xi = \tan\left(\frac{R_l}{R_s}\right)$ that represents the phase-lag between the effective thermal resistance of the solid phases $R_s = \frac{1}{(1-\varepsilon) k_s}$ and of the fluid $R_l = \frac{1}{\varepsilon k_l}$.

We now want to divide Equation (36) into two equations with a first-order time derivative. To this end, we introduce new parameter changes by posing:

$$\xi_1 = R_N \cos(\xi),\ \xi_2 = R_N \cos\xi(1+\tan\xi),\ p_1 = \frac{C_{DN}}{C_{PV}},\ p_2 = \frac{C_{BS}}{C_{PV}}. \tag{40}$$

We thus obtain two new coupled equations governing the heat-flux which are:

$$\frac{\partial\Theta}{\partial\tau} - \chi + p_1\left[\left(V\frac{\partial}{\partial Y} + W\frac{\partial}{\partial Z}\right)\Theta - W\right] = M_4 p_2 \nabla^2\Theta, \tag{41}$$

$$\begin{aligned} &C_{PV}\frac{\partial\chi}{\partial\tau} + \chi + \left(1 - p_1 - \frac{1}{\xi_1}\nabla^2\right)\left[\left(V\frac{\partial}{\partial Y} + W\frac{\partial}{\partial Z}\right)\Theta - W\right] \\ &= M_4\left(1 - p_2 - \frac{1}{\xi_2}\nabla^2\right)\nabla^2\Theta. \end{aligned} \tag{42}$$

In Equation (42), the Cattaneo-Nield, Cattaneo-Vadasz and Cattaneo-Straughan numbers can be given early in new expressions.

3. Linear Stability Analysis

To study stability exchange, we use the following double Fourier series representation for the dimensionless variables that characterize our system:

$$V(\tau,Y,Z) = -\frac{\delta^2 p_2\sqrt{2}}{\kappa p_1}\mathcal{A}e^{i\omega\tau}\cos(\kappa Y)\sin(\pi Z), \tag{43}$$

$$W(\tau,Y,Z) = \frac{\delta^2 p_2\sqrt{2}}{\pi p_1}\mathcal{A}e^{i\omega\tau}\cos(\kappa Y)\sin(\pi Z), \tag{44}$$

$$\Theta(\tau,Y,Z) = \frac{\sqrt{2}}{\pi R_f}\mathcal{B}e^{i\omega\tau}\cos(\kappa Y)\sin(\pi Z), \tag{45}$$

$$\chi(\tau,Y,Z) = \frac{\delta^2 p_2\sqrt{2}}{\pi R_f}\mathcal{D}e^{i\omega\tau}\cos(\kappa Y)\sin(\pi Z). \tag{46}$$

with

$$R_f = \frac{Ra_f\kappa^2}{\delta^4},\ \delta^2 = \kappa^2 + \pi^2. \tag{47}$$

By substituting Equation (43) to Equation (46) into Equations (33), (41) and (42), multiplying them by the orthogonal eigenfunctions, by integrating over the spatial domain, we obtain the following equations:

$$\begin{cases} -\left[\left(\dfrac{2i\omega M_0 M_1}{Va}\right) - \left(\dfrac{M_1\omega}{Va}\right)^2 + M_0^2 + M_1^2 T_f\right]\mathcal{A} + M_3\left(\dfrac{p_1}{p_2}\right)\left(\dfrac{i\omega M_1}{Va} + M_0\right)\mathcal{B} = 0, \\ R_f\mathcal{A} - \left(M_4 + \dfrac{i\omega}{\delta^2 p_2}\right)\mathcal{B} + \mathcal{D} = 0, \\ -R_f p_3\mathcal{A} + M_4 p_4\mathcal{B} - (i\omega C_{PV} + 1)\mathcal{D} = 0, \end{cases} \tag{48}$$

with

$$p_3 = \frac{p_1 - 1}{p_1} - \frac{\delta^2}{\xi_1 p_1},\ p_4 = \frac{p_2 - 1}{p_2} - \frac{\delta^2}{\xi_2 p_2},\ T_f = \frac{\pi^2 Ta}{\delta^2}. \tag{49}$$

Using the determinant method, we can solve the system (48) to obtain a non-trivial solution that corresponds to the expression of the rescaled oscillatory Rayleigh number. In fact, we have:

$$\begin{vmatrix} -\left[\left(\frac{2i\omega M_0 M_1}{Va}\right)-\left(\frac{M_1\omega}{Va}\right)^2+M_0^2+M_1^2T_f\right] & M_3\left(\frac{p_1}{p_2}\right)\left(\frac{i\omega M_1}{Va}+M_0\right) & 0 \\ R_f & -\left(M_4+\frac{i\omega}{\delta^2 p_2}\right) & 1 \\ -R_f p_3 & M_4 p_4 & -\left(i\omega C_{PV}+1\right) \end{vmatrix}=0. \quad (50)$$

So, the rescaled oscillatory Rayleigh-Darcy number, is:

$$R_f^{osc}=\frac{\left[\frac{2i\omega M_0 M_1}{Va}-\left(\frac{M_1\omega}{Va}\right)^2+M_0^2+M_1^2T_f\right]\left[\left(M_4+\frac{i\omega}{\delta^2 p_2}\right)\left(1+i\omega C_{PV}^*\right)-M_4 p_4\right]}{M_3\left(\frac{p_1}{p_2}\right)\left(\frac{i\omega M_1}{Va}+M_0\right)\left[\left(i\omega C_{PV}\right)+\left(1-p_3\right)\right]}. \quad (51)$$

Equation (51) can be rewritten in the following form:

$$R_f^{osc}=\Delta_1+i\omega\Delta_2. \quad (52)$$

Since the scaled oscillatory Rayleigh number is a real, positive physical quantity, Δ_2 must be equal to 0 or $w=0$ for the result to be physically acceptable. Using the first condition of $\Delta_2=0$, calculating the square of the oscillatory frequency from all admissible values of the control parameters leads us to negative values of ω^2. This result proves that oscillatory convection is not possible and that only the second condition is verified. Consequently, the stability exchange principle is valid in the present problem. Replacing $w=0$ in the Equation (51), we get the rescaled stationary Rayleigh number:

$$R_f^{sta}=\frac{M_4\left(M_0^2+M_1^2T_f\right)}{M_0M_3}\frac{p_2\left(1-p_4\right)}{p_1\left(1-p_3\right)}. \quad (53)$$

The stationary Darcy-Rayleigh number of the nanoliquid is then given by the expression:

$$Ra_D^{sta}=\frac{\delta^4}{\kappa^2}\left[\frac{M_4}{M_0M_3}\left(M_0^2+\frac{\pi^2 TaM_1^2}{\delta^2}\right)\right]\left[\frac{\xi_1\left(\xi_2+\delta^2\right)}{\xi_2\left(\xi_1+\delta^2\right)}\right]. \quad (54)$$

For minimality of the Darcy-Rayleigh number, differentiating Ra_{Df} with respect to κ and then assign it to 0, to yield a critical value of the wave number and substituting this value of *a* in (53) to obtain a minimal value of Darcy-Rayleigh number for the initiation of stationary convection. We have found that the value of Darcy-Rayleigh quotient alters via the factor $\frac{M_4}{M_0M_3}\left(M_0^2+\frac{\pi^2 TaM_1}{\delta^2}\right)$. In absence of nano-fragments ($\varphi=0$), M_1, M_2, M_3 and M_4 are all equal to 1. And the above condition reduces to stationary thermal Dary-Rayleigh number for simple viscous fluid convection with LTNE flux law, which absolutely agrees with those of Siddheshwar in [29] without magnetic field and rotation force.

4. Weakly Non-Linear Stability Analysis

Double Fourier expansion helps to formulate a coupled set of ODEs from the actual flow equations, which are generally proposed in the PDE formats. It is an interesting accessory for the dynamical evolution of convective flow problems under low-dimensional estimations. The flow quantities V, W, Θ and χ, as an expanded series of double-Fourier modes:

$$V(\tau,Y,Z)=-\frac{\delta^2 p_2\sqrt{2}}{\kappa p_1}\mathcal{A}(\tau)\cos(\kappa Y)\sin(\pi Z), \tag{55}$$

$$W(\tau,Y,Z)=\frac{\delta^2 p_2\sqrt{2}}{\pi p_1}\mathcal{A}(\tau)\cos(\kappa Y)\sin(\pi Z), \tag{56}$$

$$\Theta(\tau,Y,Z)=\frac{\sqrt{2}}{\pi R_f}\mathcal{B}(\tau)\cos(\kappa Y)\sin(\pi Z)-\frac{1}{\pi R_f}\mathcal{C}(\tau)\sin(2\pi Z), \tag{57}$$

$$\chi(\tau,Y,Z)=\frac{\delta^2 p_2\sqrt{2}}{\pi R_f}\mathcal{D}(\tau)\cos(\kappa Y)\sin(\pi Z)-\frac{\delta^2 p_2}{\pi R_f}\mathcal{E}(\tau)\sin(2\pi Z). \tag{58}$$

By substituting Equation (55) to Equation (58) into Equations (33), (41) and (42), multiplying them by the orthogonal eigenfunctions associated with the considered double-Fourier series expansion, by integrating over the spatial domain, we get the following equations:

$$\begin{cases}
\dfrac{\mathrm{d}\mathcal{A}}{\mathrm{d}\tau^*}=\mathcal{F}\\
\dfrac{\mathrm{d}\mathcal{B}}{\mathrm{d}\tau^*}=p_2\left(R_f\mathcal{A}-M_4\mathcal{B}-\mathcal{A}\mathcal{C}+\mathcal{D}\right),\\
\dfrac{\mathrm{d}\mathcal{C}}{\mathrm{d}\tau^*}=p_2\left(-\lambda M_4\mathcal{C}+\mathcal{A}\mathcal{B}+\mathcal{E}\right),\\
\dfrac{\mathrm{d}\mathcal{D}}{\mathrm{d}\tau^*}=\dfrac{1}{C_{PV}^*}\left(-p_3R_f\mathcal{A}+M_4p_4\mathcal{B}+p_5\mathcal{A}\mathcal{C}-\mathcal{D}\right)\\
\dfrac{\mathrm{d}\mathcal{E}}{\mathrm{d}\tau^*}=\dfrac{1}{C_{PV}^*}\left(-\lambda M_4p_6\mathcal{C}-p_7\mathcal{A}\mathcal{B}-p_2\mathcal{E}\right)\\
\dfrac{\mathrm{d}\mathcal{F}}{\mathrm{d}\tau^*}=\dfrac{2M_0Va^*}{M_1}\mathcal{F}+\dfrac{Va^*}{M_1}\left(p_1M_3R_f-\dfrac{M_0^2Va^*}{M_1}-Va^*M_1T_f\right)\mathcal{A}\\
\qquad\qquad-\dfrac{p_1M_3Va^*}{M_1}\left(\dfrac{Va^*M_4}{M_1}-\dfrac{M_0Va^*}{M_1p_2}\right)\mathcal{B}-\dfrac{p_1M_3Va^*}{M_1}\left(\mathcal{A}\mathcal{C}-\mathcal{D}\right).
\end{cases} \tag{59}$$

The derivatives of the modes are taken with regard to the time scale, $\tau^*=\left(\kappa^2+\pi^2\right)\tau$. $R_f=\dfrac{\kappa^2Ra_f}{\left(\kappa^2+\pi^2\right)^3}$ is the normalized value of the Rayleigh quotient and $\lambda=\dfrac{4\pi^2}{\kappa^2+\pi^2}$ is a geometrical quantity. The other parameters are expressed by:

$$p_5=\frac{p_1-1}{p_1}-\frac{(1+\lambda)\delta^2}{\xi_1p_1},\quad p_6=\frac{p_2-1}{p_2}-\frac{\lambda\delta^2}{\xi_2p_2},$$

$$p_7=\frac{p_1-1}{p_1}-\frac{\lambda\delta^2}{\xi_1p_1}C_{PV}^*=\delta^2C_{PV}\ \text{ and }\ Va^*=\frac{Va}{\delta^2}.$$

In the absence of rotation force, magnetic field ($Ha_f = 0$) and nano-fragments ($\varphi = 0$), this system (59) is converted to the system of Siddheshwar [29].

5. Numerical Study and Discussions

The Runge-Kutta method is well known for its efficiency in solving initial value problems of differential equations, and Zheng gives more details in [35]. We have used this method to construct an accurate numerical method for the system function (59). If we consider the first amplitude of the initial value of the first-order system, we obtain various forms of Runge-Kutta formulas; higher-order Runge-Kutta formulas can be obtained by choosing appropriate values for the parameters. Referring to the most commonly used Runge-Kutta formula, we obtain the following formula for the amplitude $\mathcal{A}$:

$$\begin{cases} \mathcal{A}_{\tau_{n+1}} = \mathcal{A}_{\tau_n} + \dfrac{1}{6}\left(K_1 + 2K_2 + 2K_3 + K_4\right), \\ K_{1\mathcal{A}} = h \cdot f_{\mathcal{A}}\left(\tau_n, \mathcal{A}_n, \mathcal{B}_n, \mathcal{C}_n, \mathcal{D}_n, \mathcal{E}_n, \mathcal{F}_n\right), \\ K_{2\mathcal{A}} = h \cdot f_{\mathcal{A}}\left(\tau_n + \dfrac{1}{2}h, \mathcal{A}_n + \dfrac{1}{2}K_1, \mathcal{B}_n + \dfrac{1}{2}K_1, \mathcal{C}_n + \dfrac{1}{2}K_1, \mathcal{D}_n + \dfrac{1}{2}K_1, \mathcal{E}_n + \dfrac{1}{2}K_1, \mathcal{F}_n + \dfrac{1}{2}K_1\right), \\ K_{3\mathcal{A}} = h \cdot f_{\mathcal{A}}\left(\tau_n + \dfrac{1}{2}h, \mathcal{A}_n + \dfrac{1}{2}K_2, \mathcal{B}_n + \dfrac{1}{2}K_2, \mathcal{C}_n + \dfrac{1}{2}K_2, \mathcal{D}_n + \dfrac{1}{2}K_2, \mathcal{E}_n + \dfrac{1}{2}K_2, \mathcal{F}_n + \dfrac{1}{2}K_2\right), \\ K_{4\mathcal{A}} = h \cdot f_{\mathcal{A}}\left(\tau_n + \dfrac{1}{2}h, \mathcal{A}_n + K_3, \mathcal{B}_n + K_3, \mathcal{C}_n + K_3, \mathcal{D}_n + K_3, \mathcal{E}_n + K_3, \mathcal{F}_n + K_3\right). \end{cases} \tag{60}$$

The same formula is applied to amplitudes $\mathcal{B}$, $\mathcal{C}$, $\mathcal{D}$, $\mathcal{E}$ and $\mathcal{F}$. Thus, the system (59) is solved using these 4th-order Runge-Kutta algorithms in Fortran language, and the bifurcation diagrams, Lyapunov exponent, phase space and time histories are represented. Predictions of the various possible dynamics of the system are obtained. According to the work of Houeto in [36], the chaos and regularity of a system (59) can be determined by the Lyapunov exponent defined by:

$$Lya = \lim_{\tau \to \infty} \frac{\ln \sqrt{\left(d\mathcal{A}\right)^2 + \left(d\mathcal{B}\right)^2 + \left(d\mathcal{C}\right)^2 + \left(d\mathcal{D}\right)^2 + \left(d\mathcal{E}\right)^2 + \left(d\mathcal{F}\right)^2}}{\tau} \tag{61}$$

with $d\mathcal{A}$, $d\mathcal{B}$, $d\mathcal{C}$, $d\mathcal{D}$, $d\mathcal{E}$ and $d\mathcal{F}$ the variation of $\mathcal{A}$, $\mathcal{B}$, $\mathcal{C}$, $\mathcal{D}$, $\mathcal{E}$ and $\mathcal{F}$ respectively. The system is chaotic when the largest Lyapunov exponent is positive, periodic when it is negative and quasi-periodic when it is zero. Table 1 shows the thermophysical properties of the nanoparticles and base fluid considered are taken from the work of Shilpa [37].

Table 1. Thermophysical properties of nanofragments and base liquid.

	$\rho\left(\mathrm{kg/m^3}\right)$	$k\left(\mathrm{W/m \cdot K}\right)$	$C_p\left(\mathrm{J/kg \cdot K}\right)$	$\beta\left(\mathrm{K^{-1}}\right)$	$\sigma\left(\mathrm{S/m}\right)$
Al_2O_3	3965.13	46.02	762	8×10^{-6}	10^{-10}
Tantalum	17014.22	57.44	138.1644	6.6×10^{-6}	7.7×10^{6}
Engine oil	884	0.144	1910	7×10^{-4}	4.64×10^{-6}

For the calculations, certain parameters are fixed: the thermal phase shift $\xi = 0.1$, the porosity-weighted diffusivity ratio is $V_N = 0.3$, the Rees number is $R_N = 100$, the phases-diffusivity ratio is $B_N = 0.5$ and the Vadasz number is $Va = 100$. The system was solved up to a maximum time value, limited to 210s with $\Delta\tau = 5\times10^{-3}$ s.

The stationary Rayleigh-Darcy number in Equation (54) is calculated using a code written in Fortran language, and curves showing its evolution as a function of wave number for different values of parameters and nanofragments volume fraction are presented. **Figure 1** shows the evolution of the stationary Rayleigh-Darcy number as a function of the wave number with different values of the Taylor-Darcy number for $\xi = 0$, $\varphi = 0$, $Ha_f = 0.1$, and $R_N = 100$. We note that increasing the nanofragments volume fraction leads to an increase in the thermal stationary Rayleigh-Darcy number. The same observation is made for its critical values. Thus, in the absence of a magnetic field and with no phase shift between the effective thermal resistance of the liquid and solid phases and the effective thermal resistance of the medium, the Taylor-Darcy number stabilizes engine oil flow by delaying the onset of stationary convection. **Figure 2** shows the evolution of the stationary Darcy-Rayleigh number when $Ta_D = 0.2$ with the variation of the phase shift between the two effective thermal resistances. By setting $Ta_D = 0.2$ and increasing the phase shift between the two effective thermal resistances, the critical value of the stationary Rayleigh-Darcy number decreases. The thermal phase shift, in the presence of the rotational force and in the absence of the Lorenz force, therefore, destabilizes the engine oil flow, accelerating the onset of stationary convection. **Figure 3** shows the variation in the stationary Rayleigh-Darcy number for $\xi = 0.15$, $Ta_D = 0.8$, $Ha_f = 0.2$, and $R_N = 100$. We observe that increasing the volume fraction of nanofragments increases the critical value of the stationary Rayleigh-Darcy number. Consequently, in the presence of thermal phase shift and rotational and Lorenz forces, nanoparticles stabilize engine oil flow by delaying the onset of stationary convection. **Figure 4** shows the evolution of the stationary Rayleigh-Darcy number as a function of the wave number with different parameter values: $Ha_f = 0.2$ for $\xi = 0.15$, $Ta_D = 0.2$, $\varphi = 0.02$, and $R_N = 100$. The curves show that increasing the intensity of the Lorenz force, with or without a phase shift, leads to an increase in the critical thermal Rayleigh-Darcy number. This shows that the magnetic field stabilizes the flow of the hybrid nanoliquid (engine oil + alumina/tantalum) by delaying the onset of stationary convection.

A comparative study of critical wave number and critical Rayleigh-Darcy number values is presented in **Table 2**. For the case of local thermal equilibrium, *i.e.*, $\xi \to 0$, $\forall R_N$, we found a Rayleigh-Darcy number $Ra_{Dc} = 39.4780$ for a critical wavenumber $\kappa_c = 3.1419$; this is in agreement with those found by Siddheshwar in [29]. These results demonstrate the reliability of our numerical calculations.

Bifurcation diagrams showing the maxima and minima of the amplitude $\mathcal{C}(\tau_*)$ versus the rescaled Rayleigh-Darcy number are plotted to study the various possible transitions in the system. **Figure 5** shows the bifurcation diagram

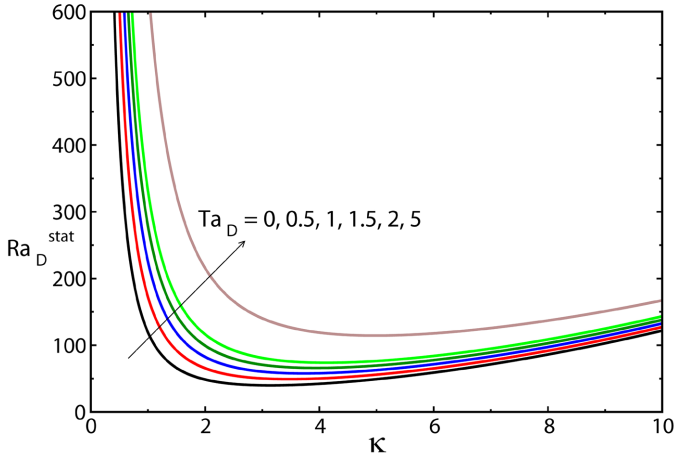

Figure 1. Stationary Rayleigh-Darcy number versus wave with different values of Ta_D number for $\xi = 0$, $\varphi = 0$, $Ha_f = 0.1$, and $R_N = 100$.

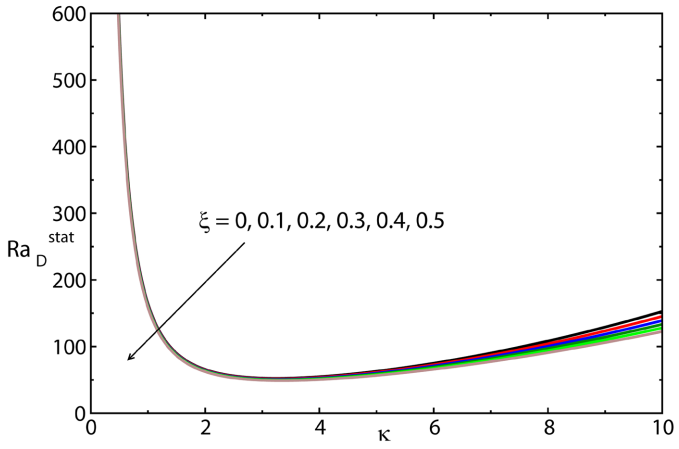

Figure 2. Stationary Rayleigh-Darcy number versus wave with different values of ξ number for $Ta_D = 0.2$, $\varphi = 0$, $Ha_f = 0.5$, and $R_N = 100$.

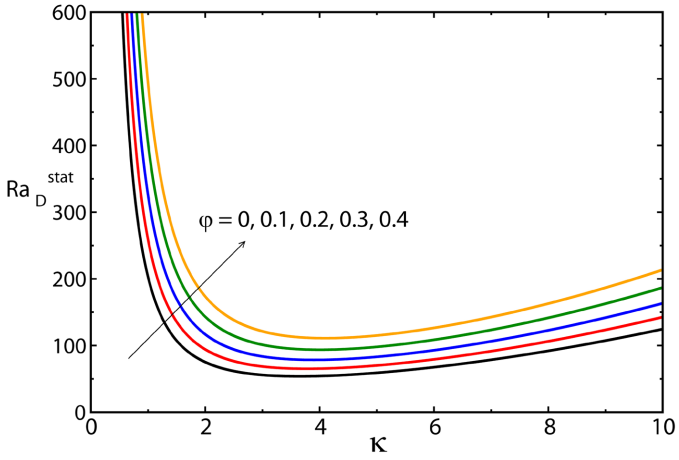

Figure 3. Stationary Rayleigh-Darcy number versus wave with different values of φ number for $\xi = 0.15$, $Ta_D = 0.8$, $Ha_f = 0.2$, and $R_N = 100$.

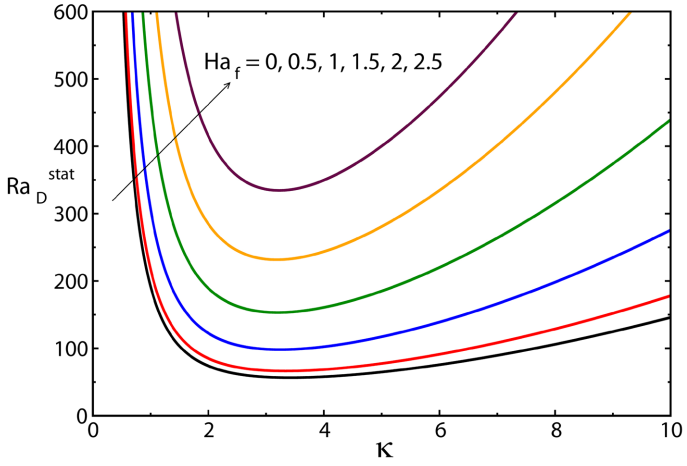

Figure 4. Stationary Rayleigh-Darcy number versus wave with different values of $Ha_f = 0.2$ number for $\xi = 0.15$, $Ta_D = 0.2$, $\varphi = 0.02$, and $R_N = 100$.

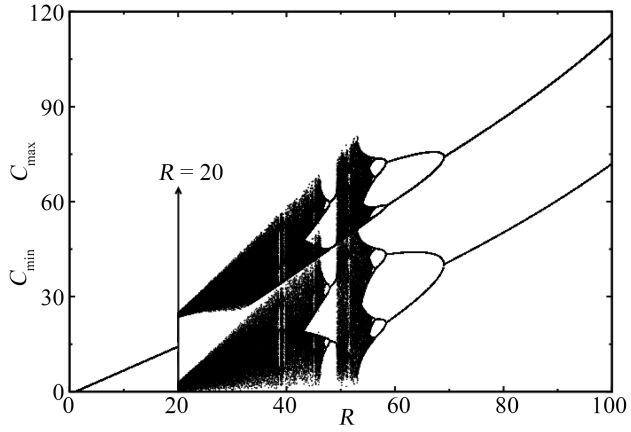

Figure 5. Bifurcation diagram of $\mathcal{C}$ as function of R for $\xi = 0.1$, $V_N = 0.3$, $\varphi_1 = \varphi_2 = 0$, $B_N = 0.5$, $Ha_f = 0.1$, $T_f = 0.1$ and $R_N = 100$.

Table 2. Critical values of wave and Rayleigh-Darcy numbers for $Ta_D = 0$, Ha_f and $\varphi = 0$.

	Siddheshwar *et al.* [29]		Present study	
Parameter Values	$B_N = 0.5$, $\xi = 0$, $R_N = 100$	$B_N = 0.5$, $\xi = 0.1$, $R_N = 100$	$\xi = 0$, $R_N = 100$	$\xi = 0.1$, $R_N = 100$,
Wave number (κ_c)	3.142	3.1521	3.1419	3.1519
Rayleigh-Darcy number (Ra_{Dc})	39.4784	39.1668	39.4780	38.88

plotted for $\varphi = 0$, $Ha_f = 0.1$ and $T_f = 0.1$. We see that the system exhibits regular, quasi-periodic or chaotic behavior marked by a continuum of points in the variable and stationary or periodic behavior with a period of one. The system characterizing the engine oil flow is found to be stationary for low rescaled Ray-

leigh-Darcy numbers, chaos appears from $R_f = 20$ with intermittent zones and has a completely regular behavior later after $R = 56$. Figure 6 shows the effect of magnetic effect on the chaotic convection in engine oil flow. When the Hartmann number is increased to $Ha_f = 0.5$, chaos starts at $R = 24.95$ and disappears completely after $R = 77$. We deduce that the magnetic field delayed the onset of turbulence in the engine oil flow as the rescaled Rayleigh-Darcy number increased. Figure 7 shows the effect of nanofragments on the dynamic behavior of the system. When the volume fraction of hybrid alumina and tantalum nanoparticles is increased to $\varphi_1 = \varphi_2 = 0.02$, the chaos starts from $R = 29.6$ and disappears completely after $R = 72.62$. Therefore, the addition of hybrid alumina and tantalum nanofragments to rotating motor oil in the presence of the magnetic field delays the onset of chaos in the flow and also reduces the chaotic domain as the thermal Rayleigh-Darcy number increases. Figure 8 and Figure 9 show the effects of nanofragments and rotation on engine flow behavior. When the volume fraction of these hybrid nanoparticles is $\varphi_1 = \varphi_2 = 0.02$ and the Taylor-Darcy number is increased to $T_f = 0.5$, the onset of chaotic convection is further delayed and the chaotic domain is enlarged.

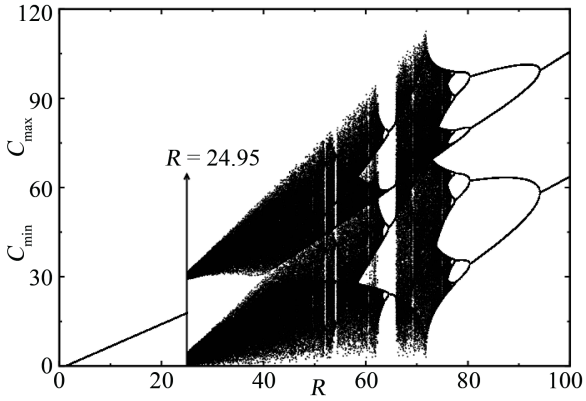

Figure 6. Bifurcation diagram of $\mathcal{C}$ as function of R for $\xi = 0.1$, $V_N = 0.3$, $\varphi_1 = \varphi_2 = 0$, $B_N = 0.5$, $Ha_f = 0.5$, $T_f = 0.1$ and $R_N = 100$.

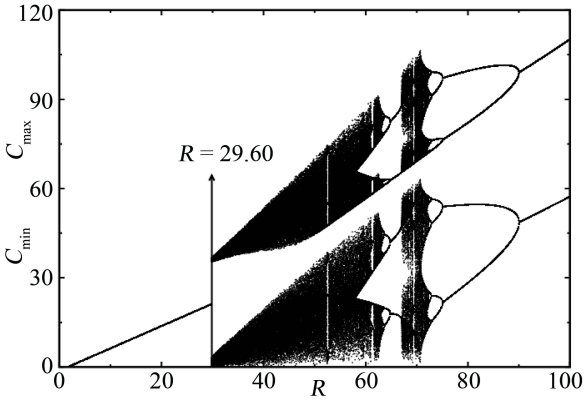

Figure 7. Bifurcation diagram of $\mathcal{C}$ as function of R for $\xi = 0.1$, $V_N = 0.3$, $\varphi_1 = \varphi_2 = 0.02$, $B_N = 0.5$, $Ha_f = 0.5$, $T_f = 0.1$ and $R_N = 100$.

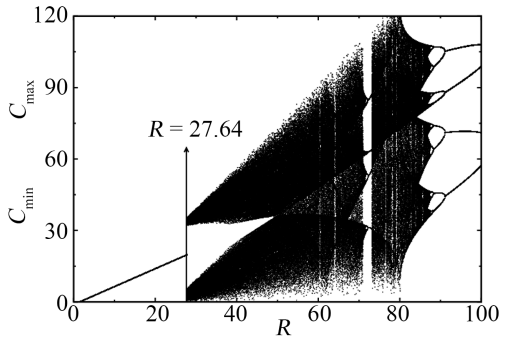

Figure 8. Bifurcation diagram of $\mathcal{C}$ as function of R for $\xi = 0.1$, $V_N = 0.3$, $\varphi_1 = \varphi_2 = 0$, $B_N = 0.5$, $Ha_f = 0.1$, $T_f = 0.5$ and $R_N = 100$.

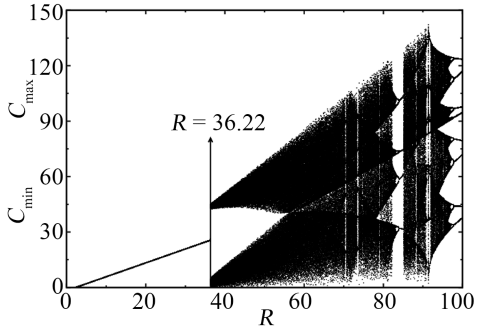

Figure 9. Bifurcation diagram of $\mathcal{C}$ as function of R for $\xi = 0.1$, $V_N = 0.3$, $\varphi_1 = \varphi_2 = 0.02$, $B_N = 0.5$, $Ha_f = 0.1$, $T_f = 0.5$ and $R_N = 100$.

Phase spaces and time evolutions are constructed to highlight and confirm some of the transition regimes that can occur in the system. To this end, **Figures 10-13** show chaotic, periodic-3, periodic-2 and periodic-1 behavior respectively. **Figure 14** shows phase spaces of the system in plane $(\mathcal{A}, \mathcal{E})$ to visualize the flow behavior for different values of volume fraction and magnetic field strength. It appears that the flow of the hybrid nanoliquid (alumina-tantalum)/engine oil can be controlled according to parameter values and desired behavior.

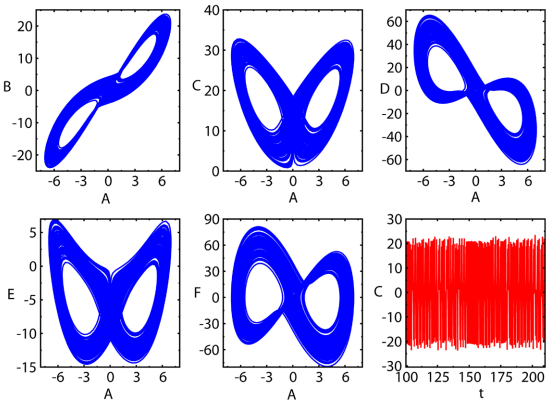

Figure 10. Phase portrait on different planes and corresponding time histories for $\xi = 0.1$, $V_N = 0.3$, $\varphi_1 = \varphi_2 = 0$, $B_N = 0.5$, $Ha_f = 0.1$, $T_f = 0.1$, $R_N = 100$ and $R_f = 25$.

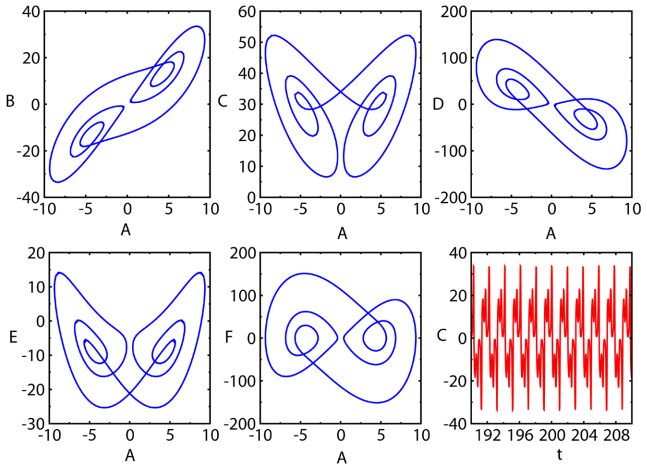

Figure 11. Phase portrait on different planes and corresponding time histories for $\xi = 0.1$, $V_N = 0.3$, $\varphi_1 = \varphi_2 = 0$, $B_N = 0.5$, $Ha_f = 0.1$, $T_f = 0.1$, $R_N = 100$ and $R_f = 38.8$.

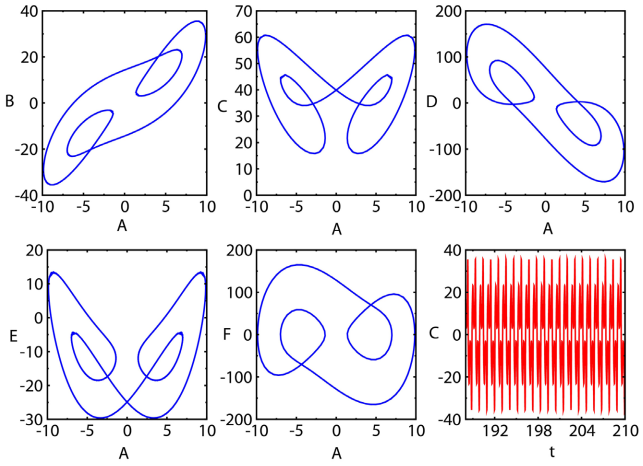

Figure 12. Phase portrait on different planes and corresponding time histories for $\xi = 0.1$, $V_N = 0.3$, $\varphi_1 = \varphi_2 = 0$, $B_N = 0.5$, $Ha_f = 0.1$, $T_f = 0.1$, $R_N = 100$ and $R_f = 48.6$.

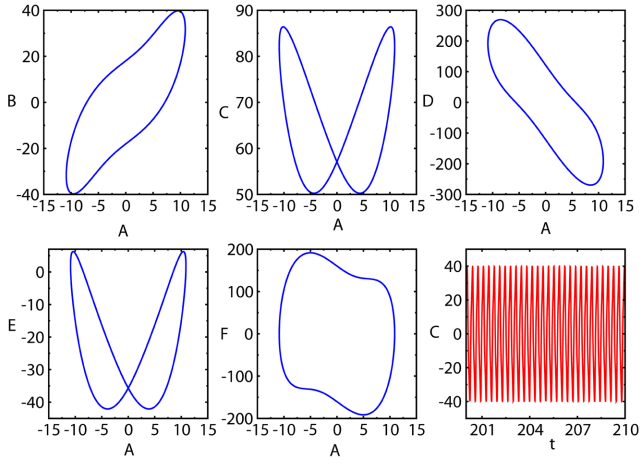

Figure 13. Phase portrait on different planes and corresponding time histories for $\xi = 0.1$, $V_N = 0.3$, $\varphi_1 = \varphi_2 = 0$, $B_N = 0.5$, $Ha_f = 0.1$, $T_f = 0.1$, $R_N = 100$ and $R_f = 80$.

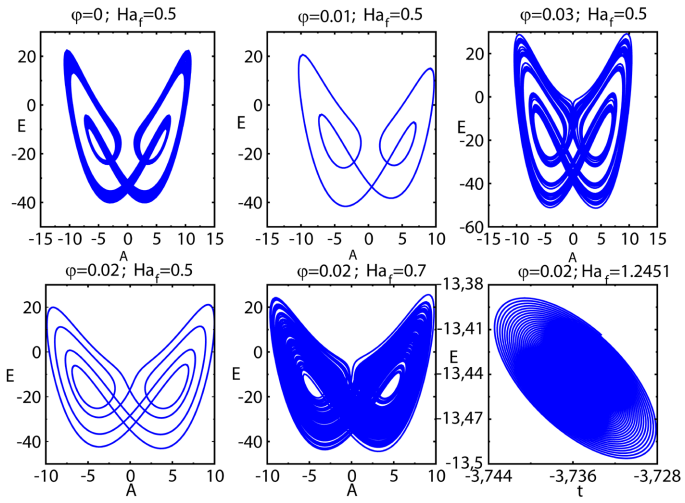

Figure 14. Phase portrait on plane $(\mathcal{A},\mathcal{E})$ for $R=61.3$, $\xi=0.1$, $V_N=0.3$, $B_N=0.5$, $T_f=0.1$ and $R_N=100$.

6. Conclusion and Suggestions

A new non-local thermal equilibrium formulation is used to evaluate the thermal and dynamic behavior of a motor oil flow confined in a porous enclosure and subjected to rotational and Lorenz forces. Indeed, the expression of the stationary thermal Rayleigh-Darcy number was found as a function of the parameters characterizing the motor oil flow and the thermophysical properties of the hybrid nanofragments. We found that the magnetic field, the rotational force and the hybrid nanofragments of alumina and tantalum delayed the onset of stationary convection in the engine oil flow. In contrast, the local thermal non-equilibrium parameter had the opposite effect on the onset of stationary convection. In addition, a new 6-dimensional nonlinear system was obtained using a low-order approach, and its numerical analysis revealed that the application of a magnetic field and a rotational force delays the onset of chaotic convection in the engine oil flow. The addition of alumina-tantalum hybrid nanoparticles to engine oil flow repels chaos and reduces the persistence of chaotic behavior in engine oil flow as the thermal Rayleigh number increases. Finally, magnetic field, rotation and nanoparticles can be used to control the dynamic behavior of the engine oil flow according to the desired result. The resulting dynamical system presents some very interesting phenomena and motivates further research into the stability of equilibrium points and the possible existence of hysteresis and attractor coexistence.

Acknowledgements

The authors would like to thank the reviewers of this paper for their valuable contributions.

Conflicts of Interest

The authors declare that there are no conflicts of interest in relation to the content

of this article.

References

[1] Zada, L., Ullah, I., Alqahtani, A.M., Nawaz, R., Khan, H. and Alam, K. (2024) Enhancing Energy Efficiency and Heat Transfer Performance of Engine Oil Flow through Hybrid Nanoparticles in Convergent/Divergent Channel. *Results in Engineering*, **22**, Article 102027. https://doi.org/10.1016/j.rineng.2024.102027

[2] Ahmad, S., Ali, K., Nisar, K.S., Faridi, A.A., Khan, N., Jamshed, W., *et al.* (2021) Features of Cu and TiO_2 in the Flow of Engine Oil Subject to Thermal Jump Conditions. *Scientific Reports*, **11**, Article No. 19592. https://doi.org/10.1038/s41598-021-99045-x

[3] Wang, F., Sohail, M., Nazir, U., El-Zahar, E.R., Singh, M., Singh, A., *et al.* (2023) Applications of Triadic Hybridized-Cross Nanomaterials Suspended in Engine Oil Using Quadratic and Linear Convection with Magnetic Dipole. *Case Studies in Thermal Engineering*, **44**, Article 102873. https://doi.org/10.1016/j.csite.2023.102873

[4] Afzal, S., Qayyum, M., Akgül, A. and Hassan, A.M. (2023) Heat Transfer Enhancement in Engine Oil Based Hybrid Nanofluid through Combustive Engines: An Entropy Optimization Approach. *Case Studies in Thermal Engineering*, **52**, Article 103803. https://doi.org/10.1016/j.csite.2023.103803

[5] Ayed, S.K., Živković, P., Tomić, M., Dobrnjac, M., Brankovi, J. and Ilić, G. (2018) Experimental Study Rayleigh-Bénard Convection in a Rectangular Motor Oil Tank. *Annals of the Faculty of Engineering Hunedoara*, **16**, 113-116.

[6] Živković, P., Tomic, M., Ayed, S.K., Barz, C. and Sever, D. (2023) Experimental and Numerical Investigation of Rayleigh-Bénard Convection in Rectangular Cavity with Motor Oil. *Thermal Science*, **27**, 216-216. https://doi.org/10.2298/TSCI230607216Z

[7] Tayebi, T. and Chamkha, A.J. (2021) Analysis of the Effects of Local Thermal Non-Equilibrium (LTNE) on Thermo-Natural Convection in an Elliptical Annular Space Separated by a Nanofluid-Saturated Porous Sleeve. *International Communications in Heat and Mass Transfer*, **129**, Article 105725. https://doi.org/10.1016/j.icheatmasstransfer.2021.105725

[8] Katto, Y. and Masuoka, T. (1967) Criterion for Onset of Convection in a Saturated Porous Medium. *International Journal of Heat & Mass Transfer*, **10**, 297-309. https://doi.org/10.1016/0017-9310(67)90147-0

[9] Morrison, H.L., Rogers, F.T. and Horton, C.W. (1949) Convection Currents in Porous Media: II. Observation of Conditions at Onset of Convection. *Journal of Applied Physics*, **20**, 1027-1029. https://doi.org/10.1063/1.1698267

[10] Horton, C.W. and Rogers, F.T. (1945) Convection Currents in a Porous Medium. *Journal of Applied Physics*, **16**, 367-370. https://doi.org/10.1063/1.1707601

[11] Straughan, B. (2001) A Sharp Nonlinear Stability Threshold in Rotating Porous Convection. *Proceedings of the Royal Society of London. Series A: Mathematical, Physical and Engineering Sciences*, **457**, 87-93. https://doi.org/10.1098/rspa.2000.0657

[12] Masuoka, T., Rudraiah, N. and Siddheshwar, P.G. (2003) Nonlinear Convection in Porous Media: A Review. *Journal of Porous Media*, **6**, 1-32. https://doi.org/10.1615/jpormedia.v6.i1.10

[13] Vadasz, P. (1999) Local and Global Transitions to Chaos and Hysteresis in a Porous Layer Heated from Below. *Transport in Porous Media*, **37**, 213-245. https://doi.org/10.1023/a:1006658726309

[14] Turkyilmazoglu, M. and Siddiqui, A.A. (2023) The Instability Onset of Generalized

Isoflux Mean Flow Using Brinkman-Darcy-Bénard Model in a Fluid Saturated Porous Channel. *International Journal of Thermal Sciences*, **188**, Article 108249. https://doi.org/10.1016/j.ijthermalsci.2023.108249

[15] Turkyilmazoglu, M. (2023) A Two-Parameter Family of Basic State in Porous Media Leading to Darcy-Bénard Convection. *Transport in Porous Media*, **148**, 519-533. https://doi.org/10.1007/s11242-023-01957-x

[16] Straughan, B. and Franchi, F. (1984) Bénard Convection and the Cattaneo Law of Heat Conduction. *Proceedings of the Royal Society of Edinburgh: Section A Mathematics*, **96**, 175-178. https://doi.org/10.1017/s0308210500020564

[17] Joseph, D.D. and Preziosi, L. (1989) Heat Waves. *Reviews of Modern Physics*, **61**, 41-73. https://doi.org/10.1103/revmodphys.61.41

[18] Christov, C.I. and Jordan, P.M. (2005) Heat Conduction Paradox Involving Second-Sound Propagation in Moving Media. *Physical Review Letters*, **94**, Article 154301. https://doi.org/10.1103/physrevlett.94.154301

[19] Christov, C.I. (2009) On Frame Indifferent Formulation of the Maxwell-Cattaneo Model of Finite-Speed Heat Conduction. *Mechanics Research Communications*, **36**, 481-486. https://doi.org/10.1016/j.mechrescom.2008.11.003

[20] Straughan, B. (2010) Thermal Convection with the Cattaneo-Christov Model. *International Journal of Heat and Mass Transfer*, **53**, 95-98. https://doi.org/10.1016/j.ijheatmasstransfer.2009.10.001

[21] Straughan, B. (2010) Porous Convection with Cattaneo Heat Flux. *International Journal of Heat and Mass Transfer*, **53**, 2808-2812. https://doi.org/10.1016/j.ijheatmasstransfer.2010.02.017

[22] Straughan, B. (2013) Porous Convection with Local Thermal Non-Equilibrium Temperatures and with Cattaneo Effects in the Solid. *Proceedings of the Royal Society A: Mathematical, Physical and Engineering Sciences*, **469**, Article 20130187. https://doi.org/10.1098/rspa.2013.0187

[23] Dehghan, M., Jamal-Abad, M.T. and Rashidi, S. (2014) Analytical Interpretation of the Local Thermal Non-Equilibrium Condition of Porous Media Imbedded in Tube Heat Exchangers. *Energy Conversion and Management*, **85**, 264-271. https://doi.org/10.1016/j.enconman.2014.05.074

[24] Shi, W., Wang, Q., Klepikova, M. and Zhan, H. (2024) New Criteria to Estimate Local Thermal Nonequilibrium Conditions for Heat Transport in Porous Aquifers. *Water Resources Research*, **60**, WR037382. https://doi.org/10.1029/2024wr037382

[25] Al-Sumaily, G.F., Al Ezzi, A., Dhahad, H.A., Thompson, M.C. and Yusaf, T. (2021) Legitimacy of the Local Thermal Equilibrium Hypothesis in Porous Media: A Comprehensive Review. *Energies*, **14**, Article 8114. https://doi.org/10.3390/en14238114

[26] Prasannakumara, B.C. (2021) Assessment of the Local Thermal Non-Equilibrium Condition for Nanofluid Flow through Porous Media: A Comparative Analysis. *Indian Journal of Physics*, **96**, 2475-2483. https://doi.org/10.1007/s12648-021-02216-9

[27] Agarwal, S. and Bhadauria, B.S. (2015) Thermal Instability of a Nanofluid Layer under Local Thermal Non-Equilibrium. *Nano Convergence*, **2**, Article No. 6. https://doi.org/10.1186/s40580-014-0037-z

[28] Kasaeian, A., Daneshazarian, R., Mahian, O., Kolsi, L., Chamkha, A.J., Wongwises, S., *et al.* (2017) Nanofluid Flow and Heat Transfer in Porous Media: A Review of the Latest Developments. *International Journal of Heat and Mass Transfer*, **107**, 778-791. https://doi.org/10.1016/j.ijheatmasstransfer.2016.11.074

[29] Siddheshwar, P.G., Kanchana, C. and Laroze, D. (2021) A Study of Darcy-Bénard

Regular and Chaotic Convection Using a New Local Thermal Non-Equilibrium Formulation. *Physics of Fluids*, **33**, Article 044107. https://doi.org/10.1063/5.0046358

[30] Dèdèwanou, S.J., Monwanou, A.V., Koukpémèdji, A.A., Hinvi, A.L., Miwadinou, C.H. and Chabi Orou, J.B. (2022) Thermal Convective Instabilities and Chaos in a Rotating Hybrid Nanofluid Layer with Cattaneo-Christov Heat Flux Model. *Complexity*, **2022**, Article ID: 9084394. https://doi.org/10.1155/2022/9084394

[31] Dèdèwanou, S.J., Hinvi, A.L., Miwadinou, H.C., Monwanou, A.V. and Orou, J.B.C. (2021) Chaotic Convection in a Horizontal Cavity Filled with (Alumina-Copper)/Water Hybrid Nanofluid Heated from Below in Presence of Magnetic Field. *Brazilian Journal of Physics*, **51**, 1079-1095. https://doi.org/10.1007/s13538-021-00929-0

[32] Cimpean, D.S., Sheremet, M.A. and Pop, I. (2020) Mixed Convection of Hybrid Nanofluid in a Porous Trapezoidal Chamber. *International Communications in Heat and Mass Transfer*, **116**, Article 104627. https://doi.org/10.1016/j.icheatmasstransfer.2020.104627

[33] Manjunatha, N., Reddy, M.G., Aloqaily, A., Aljohani, S., Reddy, A.R., Ali, F., *et al.* (2025) Radiation Effects on Rotating System Free Convective Nanofluid Unsteady Flow with Heat Source and Magnetic Field. *Partial Differential Equations in Applied Mathematics*, **13**, Article 101083. https://doi.org/10.1016/j.padiff.2025.101083

[34] Umavathi, J.C. and Bég, O.A. (2020) Modeling the Onset of Thermosolutal Convective Instability in a Non-Newtonian Nanofluid-Saturated Porous Medium Layer. *Chinese Journal of Physics*, **68**, 147-167. https://doi.org/10.1016/j.cjph.2020.09.014

[35] Zheng, L. and Zhang, X. (2017) Numerical Methods. In: Zheng, L. and Zhang, X., Eds., *Modeling and Analysis of Modern Fluid Problems*, Elsevier, 361-455. https://doi.org/10.1016/b978-0-12-811753-8.00008-6

[36] Houeto, J.G., Tokpohozin, B.N., Miwadinou, C.H., Koukpemedji, A.A. and Monwanou, A.V. (2025) Chaotic and Coexistence Attractors of Classical Complex Exotic Oscillator with Position-Dependent Mass. *International Journal of Physics*, **13**, 1-10. https://doi.org/10.12691/ijp-13-1-1

[37] Shilpa, B., Chohan, J.S., Beemkumar, N., Kulshreshta, A., Ghodhbani, R., Othman, N.A., *et al.* (2025) A Novel Machine Learning Approach for Numerical Simulation on the Hybrid Nanofluid Flow Past a Converging/Diverging Channel: Properties of Tantalum and Alumina Nanoparticles. *Partial Differential Equations in Applied Mathematics*, **13**, Article 101063. https://doi.org/10.1016/j.padiff.2024.101063